

Restricting Conformational Space: A New Blueprint for Electrically Switchable Self-Assembled Monolayers

Peer Kirsch,* Julian M. Dlugosch, Takuya Kamiyama, Christian Pfeiffer, Henning Seim, Sebastian Resch, Frank Voges, Itai Lieberman, Abin Nas Nalakath, Yangbiao Liu, Michael Zharnikov, and Marc Tornow*

Tunnel junctions comprising self-assembled monolayers (SAMs) from liquid crystal-inspired molecules show a pronounced hysteretic current–voltage response, due to electric field-driven dipole reorientation in the SAM. This renders these junctions attractive device candidates for emerging technologies such as in-memory and neuromorphic computing. Here, the novel molecular design, device fabrication, and characterization of such resistive switching devices with a largely improved performance, compared to the previously published work are reported. Those former devices suffer from a stochastic switching behavior limiting reliability, as well as from critically small read-out currents. The present progress is based on replacing Al/AIO_x with TiN as a new electrode material and as a key point, on redesigning the active molecular material making up the SAM: a previously present, flexible aliphatic moiety has been replaced by a rigid aromatic linker, thereby introducing a molecular “ratchet”. This restricts the possible molecular conformations to only two major states of opposite polarity. The above measures have resulted in an increase of the current density by five orders of magnitude as well as in an ON/OFF conductance ratio which is more than ten times higher than the individual scattering ranges of the high and low resistance states.

consumption. It is expected to use $\approx 20\%$ of the total electricity production until 2030, thus contributing significantly to global warming.^[1] In order to create an environmentally more sustainable ITC platform, a transition to new, more energy-efficient computational architectures is needed. One of the most promising alternative paradigms is neuromorphic computing,^[2] electronic circuits inspired by biological neural systems. The human brain has an energy consumption of ≈ 20 W whereas its emulation by a von Neumann supercomputer is estimated to use 1 TW,^[3] i.e., 11 orders of magnitude more. For the technical realization of neuromorphic systems new device types based on memristive materials^[4] are among the most promising candidates. Most of the active material classes currently under investigation for practical use are inorganic ones. Common mechanisms exploited to build memristive devices are filament formation, ferroelectricity, or switching between amorphous and crystalline phases.^[5,6] Also organic memristors have been reported, while so far these are mostly based on ferroelectric polymers^[7] or redox-active self-assembled monolayers (SAM).^[8]


1. Introduction

The current Internet and Telecommunication (ITC) infrastructure has become one of the major drivers of global energy

P. Kirsch, H. Seim, S. Resch, F. Voges, I. Lieberman
Merck Electronics KGaA
Frankfurter Str. 250, D-64293 Darmstadt, Germany
E-mail: peer.kirsch@merckgroup.com

P. Kirsch, A. N. Nalakath
Institute of Materials Science
Technical University of Darmstadt
Peter-Grünberg-Str. 2D, D-64287 Darmstadt, Germany

P. Kirsch
Freiburg Materials Research Center (FMF)
Albert Ludwig University Freiburg
Stefan-Meier-Str. 21, D-79104 Freiburg, Germany

 The ORCID identification number(s) for the author(s) of this article can be found under <https://doi.org/10.1002/smll.202308072>

© 2024 The Authors. Small published by Wiley-VCH GmbH. This is an open access article under the terms of the [Creative Commons Attribution License](https://creativecommons.org/licenses/by/4.0/), which permits use, distribution and reproduction in any medium, provided the original work is properly cited.

DOI: 10.1002/smll.202308072

J. M. Dlugosch, T. Kamiyama, C. Pfeiffer, M. Tornow
Molecular Electronics
Technical University of Munich
Hans-Piloty-Str. 1, D-85748 Garching, Germany
E-mail: tornow@tum.de
Y. Liu, M. Zharnikov
Angewandte Physikalische Chemie
Heidelberg University
Im Neuenheimer Feld 253, D-69120 Heidelberg, Germany
M. Tornow
Fraunhofer Institute for Electronic Microsystems and
Solid State Technologies (EMFT)
Hansastr. 27d, D-80686 Munich, Germany

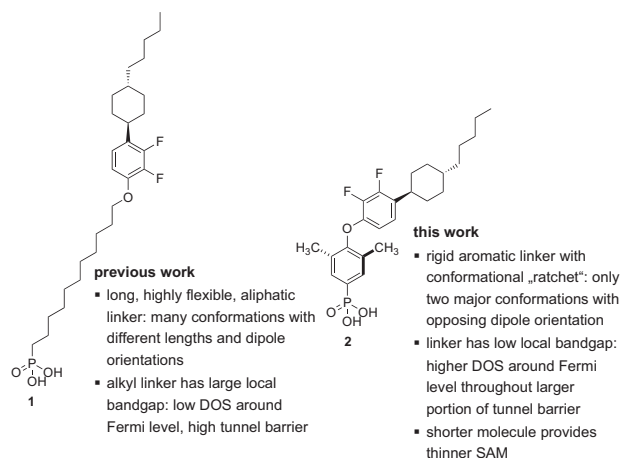


Figure 1. Previous (left) [9] and new design (right) of phosphonic acid derivatives **1** and **2** for dipolar switching in SAMs.

In our previous communication,^[9] we demonstrated the feasibility of memristive switching with liquid crystal-inspired SAMs embedded as tunnel junctions between solid-state contacts. The component molecules (**1**, **Figure 1**) are covalently anchored to the substrate by a phosphonic acid group. Their dipole moments couple to an external electrical field and changes in tunnel current are induced by a conformational reorganization and concomitant change of dipole orientation in the monolayer. This eventually results in a change of layer polarization and hence of the asymmetric tunnel barrier for the electronic charge carriers.

Although the ON/OFF ratio (ratio between conductance in the low resistive state, LRS, and the high resistive state, HRS) of **1** was measured to be quite large, in the range of 10^2 – 10^3 , the I – V curves show large scattering, which significantly reduces the reliably addressable states. This disadvantage is presumably caused by the high conformational flexibility of the long C11 linker connecting the dipolar portion of the molecule to the phosphonate anchoring group: an extremely large number of different conformations allows for a multitude of possible dipole orientations, each one with a slightly different contribution to the conductive state of the tunnel junction. Therefore, for practical applications, a limitation of conformational flexibility is needed, preferably in a system with only two major dipolar conformations. This would result in a reduction of resistance scattering between subsequent I – V cycles.

The clearer the two distinct states were separated, the higher we would also anticipate the device retention, i.e., the time during which a certain state is maintained and can be read out as often as needed. Tunnel junctions based on **1** show a retention time of the resistive states of ≈ 15 min at room temperature, which may be already sufficient for many applications in neuromorphic computing.^[6] However, a longer retention time would clearly open the technology to a broader spectrum of possible applications, including, e.g., storage class memory. In any case, both the separation of states and the retention would benefit from an increase in the activation energy barrier (E_A) for the switching between the two major dipole orientations.

Finally, besides these important device considerations, the absolute values for the current densities require attention as well:

in our previously reported ensemble molecular devices, the current densities are relatively low (e.g., in the HRS, $\approx 10^{-3}$ mA cm⁻² at ± 1 V for Al/Al₂O₃/1/Pb/Ag devices), which limits both the readout speed (due to capacitive charging effects) and a possible down-scaling of the junction area to target values in the range of 10 nm or less (absolute read-out currents would be too small: aA range). Therefore, a SAM-based device with significantly higher current density would be highly desirable, while still keeping energy consumption at tolerable values. One way to achieve higher current densities would be through an improved device architecture featuring different anchoring layers and contact materials. In fact, an increase of the current density by at least two orders of magnitude can already be observed when replacing aluminum oxide with titanium oxide (covering TiN) as the anchoring layer and replacing lead with titanium as top contact, for devices based on material **1** (see **Figure S6**, Supporting Information). To further increase current densities, careful molecular design is necessary, as a mere enrichment of the molecular backbone with conjugated moieties alone would not work: in our concept of electrically switchable tunnel junctions, the SAM components are intentionally designed with a large HOMO-LUMO gap. The switching is supposed to occur only via conformational changes in the dipolar structure but without any changes in the redox state, which might stress the organic material during prolonged and repeated operation, in effect possibly reducing the endurance of the device.

2. Results and Discussion

2.1. Molecular Design and Synthesis

One possible way to increase the efficiency of tunneling through the molecules and thus their conductivity is carefully reducing the HOMO-LUMO gap over a larger portion of the tunnel barrier, placing a higher density of accessible states closer to the molecules' Fermi level. From the viewpoint of molecular design, this can be achieved by replacing the long aliphatic linker with its large local band gap (typical HOMO-LUMO gap of alkanes ≈ 8 eV) with an aromatic moiety (estimated HOMO-LUMO gap of the 2,3-difluorophenylene moiety in **1** ≈ 5.9 eV, and ≈ 5.5 eV for the whole diaryl ether unit in **2**).^[10]

Based on all these considerations, structure **2** was specifically designed for the next generation of SAM-based, electrically switchable tunnel junctions: compared to **1**, in **2** the C11 alkylene linker is replaced by an aromatic moiety, with *ortho*-methyl groups acting as molecular ratchets, restricting the conformational flexibility to only two possible dipole orientations (see, **Figure 2**). The synthesis of **2** (**Scheme 1**) is described in more detail in the Supporting Information. As a non-polar reference compound, the non-fluorinated analog **3** (**Scheme 1**) was prepared by a similar method.

To address the major requirements listed above, we at first focused on the anticipated higher activation energy for dipolar reorientation for our newly designed compound **2**, by carrying out model calculations. In general, the energy barrier is determined by inter- as well as intramolecular interactions between or within the molecules making up the SAM, respectively. Whereas the intermolecular contribution to E_A is difficult to assess due to lack of knowledge of the exact microscopic structure of the SAM, an estimate of the intramolecular part can be obtained

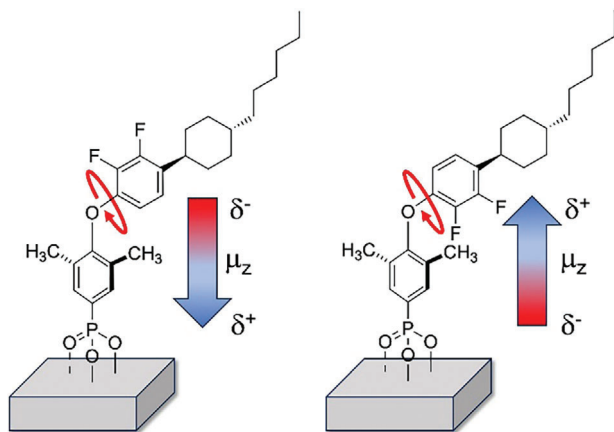
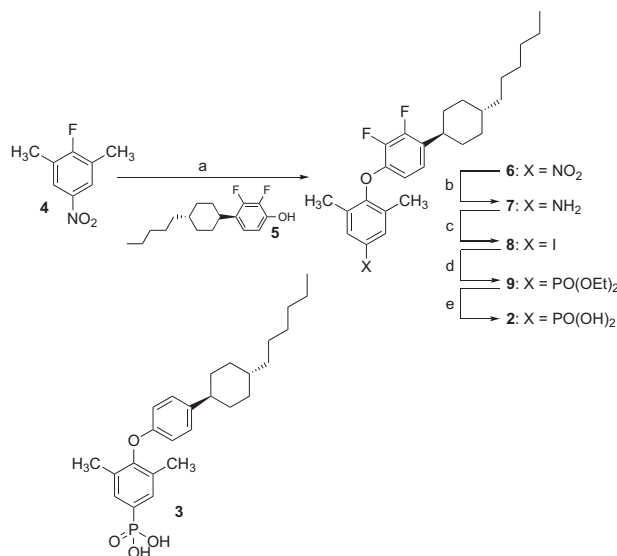


Figure 2. Illustration of the mechanism of dipolar switching of **2**: application of an external electrical field flips the polar 2,3-difluorophenylene group up (left) or down (right), resulting in different tunnel currents through the SAM.

from a simple dihedral scan for the rotation of the dipolar moiety of the molecule around the O–C_{ar} bond (**Figure 3**): at first, our computational analysis of a simplified model of molecule **1** (labeled **A** in **Figure 3**) indicates that the relevant barriers for the rotation around the COC_{ar}C_{ar} dihedral are only 1.41 kcal mol⁻¹ (from *syn* to *anti*) and 2.10 kcal mol⁻¹ (from *anti* to *syn*) – intriguingly far less than what would be required for the observed retention time of ≈15 min (estimated >20 kcal mol⁻¹).^[11a] This can only be reconciled if we assume that the effective barrier is much higher, and dominated by intermolecular interactions in the sterically crowded SAM. Also, (collective) intermolecu-



Scheme 1. Synthesis of the phosphonic acid **2**: a) **5**, K₂CO₃, DMSO; 125 °C, 18 h (87%). b) H₂, 5% Pd-C, *i*-PrOH, THF; 5 bar, room temp., 18 h (98%). c) NaNO₂, CH₂I₂, HOAc, CH₂Cl₂, H₂O; room temp., 18 h (60%). d) P(OEt)₃, cat. Pd(OAc)₂, dioxane; reflux, 75 min (87%). e) Me₃SiBr, CH₂Cl₂; room temp., 18 h (44%). The non-fluorinated reference compound **3** is synthesized by the same method using the non-fluorinated analog of **5**.

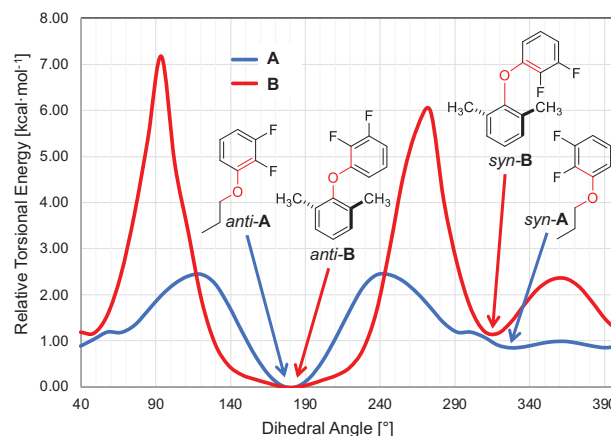


Figure 3. Calculated dihedral energy scan (M06-2X-D3/6-31G(d) level of theory; in a second step the minima and transition states were fully optimized (M06-2X-D3/6-31G(d,p) and ZPE corrected)^[10] for the dihedral rotation of the dipolar 2,3-difluorophenylene moiety against the linker unit (marked in red). For both simplified model compounds **A** (corresponds to **1**) and **B** (to **2**, respectively), for the sake of computational efficiency, the global minimum is the *anti*-conformation with a dihedral angle of 180°, in both cases energetically slightly preferred over *syn*. The relative energies of the *syn* conformers vs. *anti* are 0.69 kcal mol⁻¹ for **A** and 1.27 kcal mol⁻¹ for **B**.

lar dipole interactions might contribute to this higher effective barrier.^[11b] Then as expected, in contrast to the rather flat profile of **A**, the dihedral scan of **B** (simplified version of **2**) shows significantly higher barriers of 5.11 kcal mol⁻¹ (from *syn* to *anti*) and 6.39 kcal mol⁻¹ (from *anti* to *syn*). Both model compounds **A** and **B** show a double minimum of their *syn* conformation with the 2,3-difluorophenylene subunit slightly twisted against the alkoxy resp. aryloxy moiety. This is due to the repulsive interaction in the exact *syn*conformation between the 2-fluorine substituent and the α methylene group of the linker for **A** and the π system of the dimethyl phenylene linker in **B**. The crystal structure of **2** (see Supporting Information) shows a conformation with a dihedral angle (C21-O20-C15-C16) of 146.7(3)°, twisted by ≈35° out of the global minimum at 180°. The oxygen valence angle (C21-O20-C15) is 118.1(3)°.

2.2. SAM and Device Characterization

Next, we set out to evaluate our novel molecular design in actual monolayer memristive devices. Before the fabrication of such electrical junctions, SAMs from all compounds under study (**2**, as well as **1** and **3** – the non-fluorinated and thus practically non-polar analog of **2**) were deposited (for the protocol, see Supporting Information) on non-structured, planar TiN reference chips and investigated thoroughly with respect to their structural and surface chemical properties. In particular, X-ray photoelectron spectroscopy (XPS) data clearly verified the presence of the respective SAMs. They also indicated the presence of a layer of at least 2 nm of TiO₂ between TiN and SAM. Taking the deposition process into account, the hydrolysis and oxidation of the top layer of the TiN to TiO₂ can be chemically expected. Based on XPS, the thickness of the SAMs was estimated to be 2.4 ± 0.2 nm for **1**, and 1.60 ± 0.15 nm for both, **2** and **3**; note, however, that these values

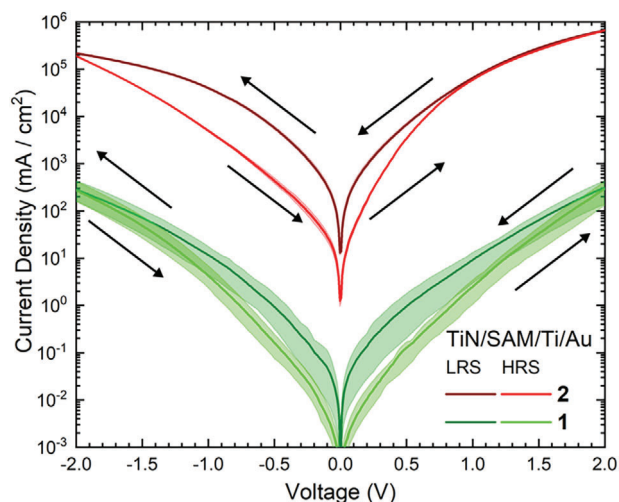


Figure 4. Current–density versus voltage characteristics of TiN/SAM/Ti/Au ($20 \times 20 \mu\text{m}^2$) junctions comprising SAMs of **2** in comparison to **1**. The J – V curves show averages from three cycles (sweeps from 0 V to +2.0 V to –2.0 V and back to 0 V, scan direction indicated by arrows) and three devices, each. The minimum and maximum current densities at each voltage are shown as envelopes, and the area between is shaded. The shaded areas of **2** are hardly visible, since their J – V traces show – in contrast to those of **1** – extremely low variability rendering the envelope nearly invisible.

represent the lowest estimates and the real thicknesses are most likely higher by 0.3–0.5 nm (see Supporting Information for details). The thickness difference between **1** and **2**, **3** is well in agreement with the expectation, based on their dissimilar molecular contour lengths (**1**: ≈ 2.8 nm, **2**: ≈ 2.0 nm), cf. Figure 1. Complementary X-ray absorption spectroscopy measurements indicate that molecules **2** and **3** have an upright orientation in the SAMs but a lower packing density as well as a lesser degree of conformational order than molecules **1** (for more details, see Supporting Information).

Subsequent to the SAM characterization, tunnel junctions with TiN as bottom electrodes and Ti (10 nm)/Au (80 nm) solid-state top contacts on the monolayers were fabricated and electrically characterized, largely following the protocol reported in Ref. [12] Here, the gold capping layer improved lateral conductivity and prevented titanium from oxidation. Details of the fabrication process including a STEM cross-sectional image of a FIB cut of the junction, confirming the SAM's integrity after top contact deposition, can be found in the Supporting Information (Figure S3, Supporting Information).

Comparison of the J – V characteristics of **1** and **2** (Figure 4) indicates an extremely low cycle-to-cycle and device-to-device variability of **2** – as intended by the molecular design. The J – V trace of its non-fluorinated, non-polar analog **3** (see Figure S7, Supporting Information), which was prepared as a reference, shows a much smaller hysteresis occurring in a different voltage range.

Further, the current density for **2** is at least 3 orders of magnitude higher than the one for **1** (at ± 1 V). As a higher current density for **2** in comparison to **1** was one of our initial molecular design targets, it should be mentioned again that also for compound **1** the current density of the TiN/1/Ti/Au device is at least two orders of magnitude higher at these read-out voltages

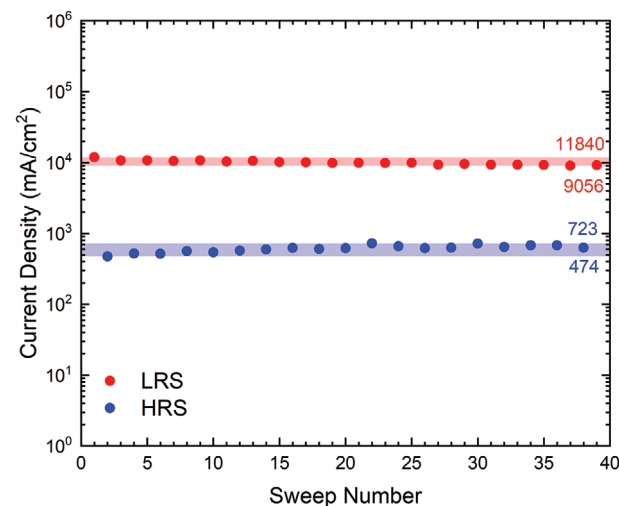
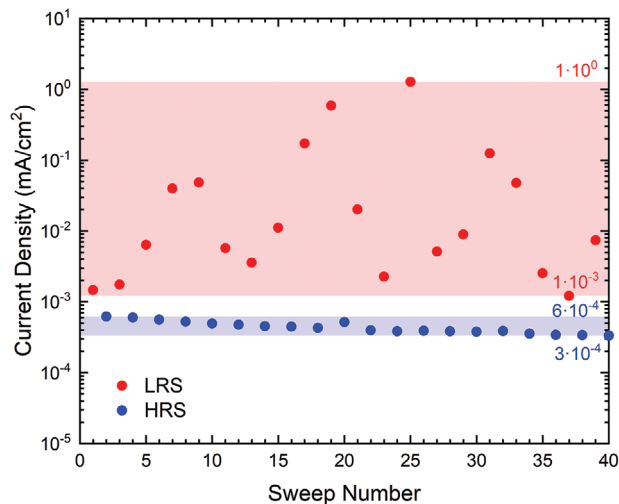


Figure 5. Current density in the HRS and LRS, as a function of sweep number (here, two sweeps make up one cycle). Top: measured at -1.0 V for compound **1** in the first-generation Al/Al₂O₃/1/Pb/Ag device stack.^[9] Bottom: at -0.45 V for compound **2** in the TiN/2/Ti/Au device stack. In both cases, the read-out voltages were chosen close to the maximum value of either ON/OFF ratio (see also Figure S8, Supporting Information), but also with sufficient current density at the selected voltage. Our previously reported system, Al/Al₂O₃/1/Pb/Ag ($25 \times 25 \mu\text{m}^2$) (Figure S6, Supporting Information), shows a large scattering of the LRS as well as a slight downward drift of the current density with successive sweeps. In contrast, the TiN/2/Ti/Au device ($5 \times 5 \mu\text{m}^2$) has a stable ON/OFF ratio of about one order of magnitude, with a low scattering of LRS and HRS.

than for the Al/Al₂O₃/1/Pb/Ag device described in our previous communication,^[9] cf. Figure S6 (Supporting Information). Presumably, this is mainly due to the absence of the insulating Al₂O₃ anchoring layer. This renders the current density of the optimized TiN/2/Ti/Au device altogether at the minimum five orders of magnitude higher than for the first, proof-of-concept device (Al/Al₂O₃/1/Pb/Ag).

This effect can be immediately discerned with the help of Figure 5, which directly compares the HRS and LRS current densities as a function of the sweep number, of one first-generation device (Al/Al₂O₃/1/Pb/Ag) with those of one new TiN/2/Ti/Au

device. Having both major improvements (molecular design and electrode material) implemented, the resulting strong increase in current density as well as the already observed, greatly enhanced state stability are evident. In fact, at the voltage with the highest average ON/OFF conductance ratio, system 1 shows a large scattering of the LRS with successive sweeps. In contrast, the novel TiN/2/Ti/Au device exhibits an excellent repeatability of its HRS and LRS with an ON/OFF ratio $J_{\text{LRS}}/J_{\text{HRS}} > 10$ for all measured 20 switching cycles – not only on average. Importantly, this ratio is also more than ten times higher than the individual scattering ranges (max/min conductance ratio) of HRS and LRS, in contrast to the first-generation device data (see, the numerical range limits included in Figure 5). As the average ON/OFF ratios for 1 and 2 are still quite comparable for the same contact materials (cf., Figure 4), we conclude that the dominating current switching mechanism is mainly related to the dipole orientation of the polar 2,3-difluorophenylene unit in both cases.

3. Conclusion

On the way toward neuromorphic devices based on molecular films, a new scaffold for the dipolar switching of SAM components was designed. Compared to the first generation, based on liquid crystal-like structures 1, the new material 2 shows a rotational energy profile with significantly stronger pronounced minima, separated by higher activation barriers. In addition, the current density through the device was significantly increased (by at least three orders of magnitude, at ± 1 V), by using a diphenyl ether backbone featuring a smaller band gap and thus a higher density of states close to the Fermi level. A further enhancement of the current density (up to at least two orders of magnitude) could be achieved by using TiN as the bottom electrode material instead of Al/Al₂O₃.

In particular for tunnel junctions, achieving a certain minimum current density of the LRS at READ voltage is mandatory for practical industrial application of the devices. Therefore, we benchmarked our device (current density of 10^4 mA cm⁻² at -0.45 V, Figure 5) against various other solid-state, ferroelectric tunnel junctions recently reported in the literature (for details, see Table S1, Supporting Information). This comparison shows that the current density of our device is in the same range as the ones of FTJs using inorganic ferroelectrics with the highest current densities reported, at comparable READ voltages.^[13] It can be up to four orders of magnitude higher than for FTJs based on ferroelectric polymer films of comparable thickness.^[7] There is currently no report on FTJs based on low-molecular-weight SAMs, to the best of our knowledge.

Finally, the most prominent feature of the new class of materials (2) is its extremely reproducible switching behavior: J - V characteristics of the new device generation show a “clean” switching between high and low resistive states, with a current ON/OFF ratio of > 10 . The noise level of the switching is very low, and the junctions show stable operation without drift over at least 20 cycles, suggesting that they could also be used in multi-level or analog memory devices in forthcoming applications.

Future work will be directed toward developing SAM-based tunnel junctions for practical applications, such as synapses in neuromorphic circuitry. This shall include an extended study and optimization of device retention, switching dynamics (time de-

pendence), and spike-time dependent state potentiation and depression (under pulsed operation).

Supporting Information

Supporting Information is available from the Wiley Online Library or from the author.

Acknowledgements

The authors thank A. Lawrence, C. Turner, E. Boreham, L. Arnold, and D. Hall (Colour Synthesis Solutions, Manchester, UK) for the synthetic work, S. Kishi (Samurai Semiconductors) for the STEM measurements, C. v. Esen (Merck KGaA) for measuring and solving the crystal structure, and N. Agourram (TU Darmstadt) for the preparation of SAM-coated TiN chips. Y.L. and M.Z. thank the Helmholtz Zentrum Berlin (HZB) for the allocation of synchrotron radiation beam time at BESSY II and financial support, S. Das for the assistance with the XPS measurements and data processing, and M. Brzhezinskaya (HZB) for technical support. Y.L. thanks the China Scholarship Council (CSC) for financial support.

Open access funding enabled and organized by Projekt DEAL.

Conflict of Interest

The authors declare no conflict of interest.

Data Availability Statement

The data that support the findings of this study are available in the supplementary material of this article.

Keywords

conformation design, dipolar switching, memristor, neuromorphic computing, tunnel effect

Received: September 14, 2023

Revised: April 18, 2024

Published online: May 2, 2024

- [1] R. Arshad, S. Zahmoor, M. A. Shah, A. Wahid, H. Yu, H. Green, *IEEE Access*. **2017**, *5*, 15667.
- [2] a) C. Mead, *IEEE*. **1990**, *78*, 1629; b) R. Yang, H.-M. Huang, X. Guo, *Adv. Electron. Mater.* **2019**, *1900287*.
- [3] L. M. Krauss, IET Blog, <http://edge.org/response-detail/26163>, (accessed: Nov 2022).
- [4] a) L. O. Chua, *IEEE Trans. Circuit Theory*. **1971**, *18*, 507; b) D. B. Strukov, G. S. Snider, D. R. Stewart, R. S. Williams, *Nature*. **2008**, *453*, 80; c) Z. Wang, H. Wu, G. W. Burr, C. S. Hwang, K. L. Wang, Q. Xia, J. J. Yang, *Nat. Rev. Mater.* **2020**, *5*, 173.
- [5] a) D. Ielmini, S. Ambrogio, *Nanotechnology*. **2019**, *31*, 092001; b) S. H. Park, H. J. Lee, M. H. Park, J. Kim, H. W. Jang, *J. Phys. D: Appl. Phys.* **2024**, *57*, 253002.
- [6] D. V. Christensen, R. Dittmann, B. Linares-Barranco, A. Sebastian, M. L. Gallo, A. Redaelli, S. Slesazek, T. Mikolajick, S. Spiga, S. Menzel, I. Valov, G. Milano, C. Ricciardi, S.-J. Liang, F. Miao, M. Lanza, T. J. Quill, S. T. Keene, A. Salleo, J. Grollier, D. Marković, A. Mizrahi, P. Yao, J. J. Yang, G. Indiveri, J. P. Strachan, S. Datta, E. Vianello, A. Valentian, J. Feldmann, et al., *Neuromorph. Comput. Eng.* **2022**, *2*, 022501.

- [7] S. Majumdar, H. Tan, Q. H. Qin, S. van Dijken, *Adv. Electron. Mater.* **2019**, *5*, 1800795.
- [8] X. Chen, M. Roemer, L. Yuan, W. Du, D. Thompson, E. del Barco, C. A. Nijhuis, *Nat. Nanotechnol.* **2017**, *12*, 797.
- [9] J. M. Dlugosch, H. Seim, A. Bora, T. Kamiyama, I. Lieberman, F. May, F. Müller-Plathe, A. Nefedov, S. Prasad, S. Resch, K. Saller, C. Seim, M. Speckbacher, F. Voges, M. Tornow, P. Kirsch, *ACS Appl. Mater. Interfaces.* **2022**, *14*, 31044.
- [10] Gaussian 16, Revision C.01, M. J. Frisch, G. W. Trucks, H. B. Schlegel, G. E. Scuseria, M. A. Robb, J. R. Cheeseman, G. Scalmani, V. Barone, G. A. Petersson, H. Nakatsuji, X. Li, M. Caricato, A. V. Marenich, J. Bloino, B. G. Janesko, R. Gomperts, B. Mennucci, H. P. Hratchian, J. V. Ortiz, A. F. Izmaylov, J. L. Sonnenberg, D. Williams-Young, F. Ding, F. Lipparini, F. Egidi, J. Goings, B. Peng, A. Petrone, T. Henderson, D. Ranasinghe, et al., Gaussian, Inc, Wallingford CT **2016**.
- [11] a) M. Oki, in *Topics in Stereochemistry*, Vol. 14, (Eds.: E. L. Eliel, N. L. Allinger, S. H. Wilen), John Wiley & Sons, New York **1983**, pp. 1–82; b) E. Zojer, T. C. Taucher, O. T. Hofmann, *Adv. Mater. Interfaces.* **2019**, *6*, 1900581.
- [12] J. M. Dlugosch, D. Devendra, D. Chryssikos, S. Artmeier, M. Speckbacher, T. Kamiyama, M. Tornow, *Proc. IEEE Conf. Nanotechnol.* **2020**, (July), 29–34, <https://doi.org/10.1109/nano47656.2020.9183521>.
- [13] S. S. Cheema, N. Shankar, C.-H. Hsu, A. Datar, J. Bae, D. Kwon, S. Salahuddin, *Adv. Electron. Mater.* **2022**, *8*, 2100499.